QUANTITATIVE SCANNING ELECTRON MICROSCOPY OF SURFACES

L. Reimer

JOURNAL DE PHYSIQUE
Colloque C2, supplément au n°2, Tome 45, février 1984

QUANTITATIVE SCANNING ELECTRON MICROSCOPY OF SURFACES

L. Reimer

Physikalisches Institut, Universität Münster, Domagkstrasse 75, D-4400 Münster, F.R.G.

Résumé - Les informations relatives à la topographie et à la composition de l'échantillon, contenues dans les images en électrons secondaires et en électrons rétrodiffusés, peuvent être quantitatives. Elles nécessitent d'être obtenues avec des détecteurs différents convenablement placés.

Abstract - The emissive modes of secondary and backscattered electrons in a scanning electron microscope work more quantitavely for material and topographic contrasts and can better separate different types of contrast when using a multi-detector system.

The detector system of conventional scanning electron microscopes often do not make the best use of the potentialities given by the electron-specimen interactions and a better detector strategy will be necessary also to get more quantitative results /1/. For example, the Everhart-Thornley detector designed for collecting as much secondary electrons (SE) as possible, only collects an undefined fraction of the emitted SE depending on the specimen position and the dimension of the specimen chamber, and a large fraction of the SE signal is formed by SE which are excited by the backscattered electrons (BSE) at the lower pole-piece and other parts of the specimen chamber. The micrographs contain an undefined mixture of topographic and material contrast. The BSE are not collected by electrostatic collection fields and it is necessary to use scintillator or semiconductor detectors with a large solid angle of collection. Therefore, experiments have been done to use BSE detectors at different positions /2-5/ and also two BSE detectors A and B for separating material and topographic contrasts with the signals A+B and A-B, respectively/6,7/. However, we show below that the A-B signal can contain image artifacts which are not caused by topography.

I - Backscattering and secondary electron emission

For a better understanding of the concepts for improving the detector strategy, the most important laws of BSE and SE emission shall be summarized /8/. The backscattering coefficient η increases monotonously with increasing atomic number Z for primary electron energies $E \geq 5$ keV (Figs. 1 and 5). Below 5 keV, η decreases for large Z /9/ which can be explained quantitatively by Monte Carlo calculations /10/ using Mott instead of Rutherford cross-sections for considering the large-angle scattering which is mainly responsible for the effect of backscattering. With increasing tilt angle ϕ the total backscattering coefficient η increases (Fig.2). When looking on the angular characteristics $d\eta/d\Omega$ (Fig.3), this increase of η with increasing ϕ is concentrated in a reflection-like maximum /11/. This increase will only be observed in the BSE signal when the detector is positioned at the corresponding take-off direction. With BSE detectors below the pole-piece, only the fraction of BSE emitted opposite to the electron beam will be collected. These BSE leave the specimen by complete diffusion. The corresponding BSE signal depends only weakly on ϕ and is approximately constant for tilt angles $\phi \leq 0\text{-}50^{\circ}$ and decreases for larger ϕ. The energy distribution

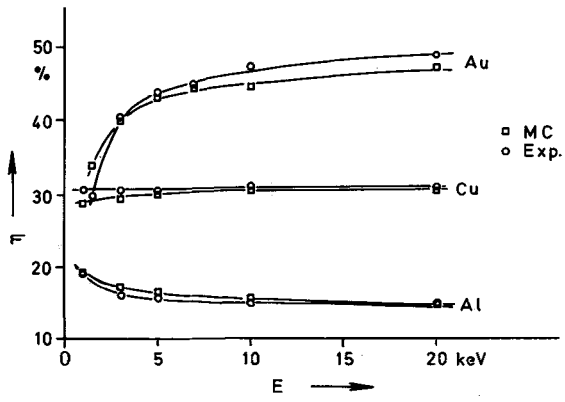

Fig.1 - Dependence of η on electron energy.

Fig.2 - Dependence of η on specimen tilt angle Ø.

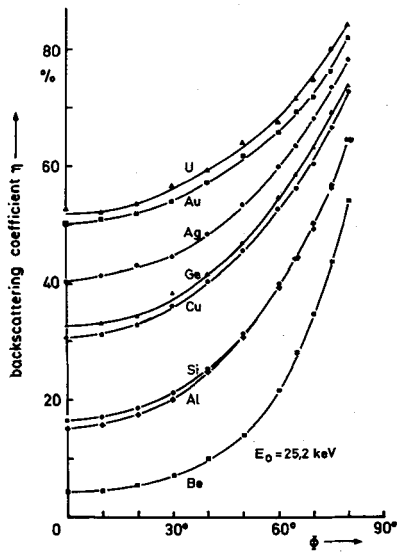

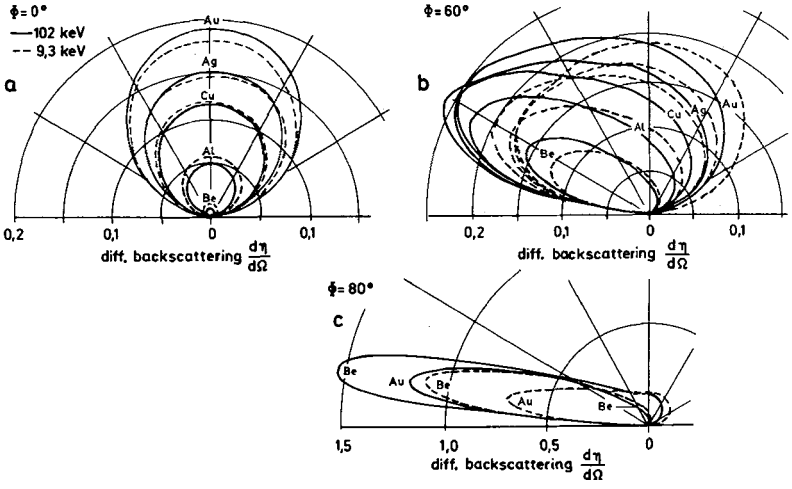

Fig.3 - Angular characteristics dη/dΩ for tilt angles Ø = 0, 60° and 80°.

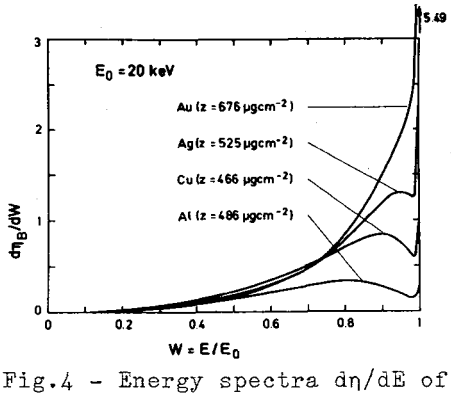

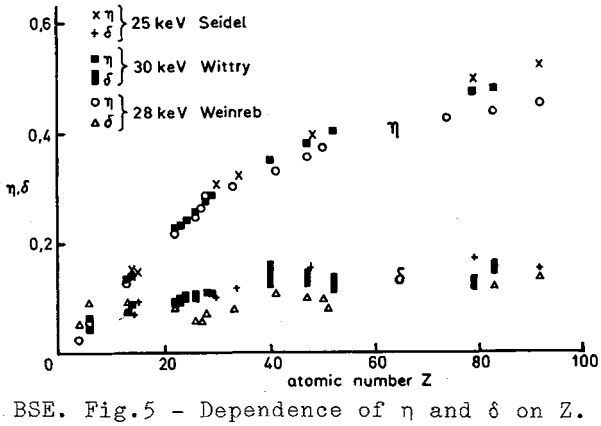

Fig.4 - Energy spectra dη/dE of BSE. Fig.5 - Dependence of η and δ on Z.

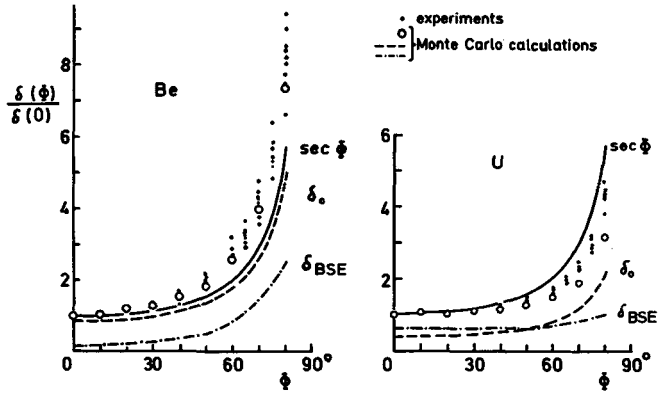

Fig.6 - Dependence of $\delta(\phi)/\delta(0)$ on the tilt angle ϕ, $\delta_o = \delta_{PE}$ contribution of the primaries, δ_{BSE} = contribution of the BSE.

of the BSE shows an elastic peak, the magnitude of which increases with decreasing electron energy and increasing tilt angle ϕ and also depends on the take-off angle /12,13/. The most probable BSE energy is shifted to lower $W = E_{BSE}/E_o$ with decreasing Z (Fig.4).

Secondary electrons are by convention electrons with exit energies below 50 eV. They can leave the specimen only from a small exit depth of the order of a few nanometres /14/. The secondary electron yield δ will be proportional to the path length of the primary electrons (PE) $\propto \sec \phi$ and the probability of ionisation which is proportional to the Bethe stopping power $S = dE/ds \propto E^{-1} \ln(E/I) \simeq E^{-0.8}$ /11/. But also the fraction η of BSE generate SE on their path through the surface and the mean number of excited SE will be a factor $\beta \simeq 2\text{-}3$ larger than the corresponding value for PE due to the decrease of $E_{BSE} < E$ and increased angles ϕ through the surface /15,16/

$$\delta = \delta_{PE} + \delta_{BSE} = \delta_o \sec \phi + \delta_o \beta \eta \quad . \qquad (1)$$

where δ_o denotes the contribution of PE to the SE yield at normal incidence (ϕ=0). The contribution δ_{BSE} results in an increase of δ with increasing Z due to the increase of η but the values show a larger scatter due to the factor δ_o which also depends on the surface contamination (Fig.5). The increase of δ with increasing ϕ (Fig.6) is only in first order proportional to sec ϕ and shows systematic differences for low and high Z material which can be explained by the contributions in (1) using a Monte Carlo program. The angular distribution $d\delta/d\Omega$ of SE can be approximated by a Lambert law

$$\frac{d\delta}{d\Omega} = \frac{\delta}{\pi} \cos \alpha \ , \qquad (2)$$

where α denotes the take-off angle relative to the surface normal. The most probable energy of the SE spectrum is of the order of 2-5 eV. For single-crystal specimens both η and δ depend on the direction of incidence relative to the lattice planes due to channelling effects of the primary Bloch-wave field /8/.

II - Material and topographic contrasts

A detector system using two opposite Everhart-Thornley detectors (ETD) for the detection of SE and BSE /17/ is shown in Fig.7. A ring electrode around or a spherical grid above the specimen stub decreases the electric field of the positively biased collector grid of the ETDs, so that SE can travel a distance due to their exit momenta until they reach the collection field and are accelerated to the detectors A or B. A positively biased copper plate below the pole-piece plate and behind an earthed grid suppresses the signal of SE which are normally excited by the BSE at the pole-piece. A negatively biased ring or grid suppresses the signal of SE from the specimen and a negatively biased copper plate emits the SE excited by the BSE. Additionally, such a BSE/SE converter

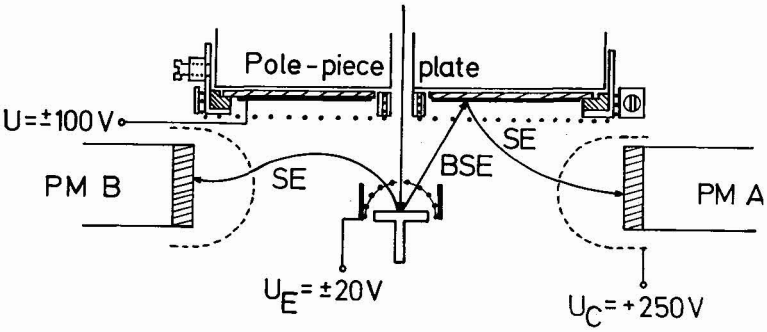

Fig.7 - Detector system of two Everhart-Thornley detectors A and B with a BSE/SE converter plate at the lower pole-piece.

plate can be coated with MgO to increase the BSE/SE conversion yield. Due to charging effects the yield is of the order of unity for all BSE energies below 20-30 keV until $\sigma=\eta+\delta<1$ with increasing E /18/.

Figure 7 shows micrographs obtained with the A+B SE and BSE modes from circonium oxide inclusions in a glass matrix. The specimen is mechanically polished and coated with a thin gold film to prevent charging. Both A+B SE and BSE micrographs (a,c) show material contrast, the former due to the contribution δ_{BSE} in equ. (1) and the increase of δ with increasing Z (Fig.5). This material contrast is cancelled in the A-B modes (b,d). However, whereas the A-B SE mode (b) represents the true surface topography, the A-B BSE mode (d) not only shows less resolution due to the larger information depth but also a characteristic image artifact which improves an expression of a surface step between circonium oxide and glass. This image artifact was also found for eutectic alloys and also with semiconductor detectors /7/. Figure 8 demonstrates by Monte Carlo calculations how different signal amplitudes A and B and a non-vanishing A-B signal result when scanning across a phase

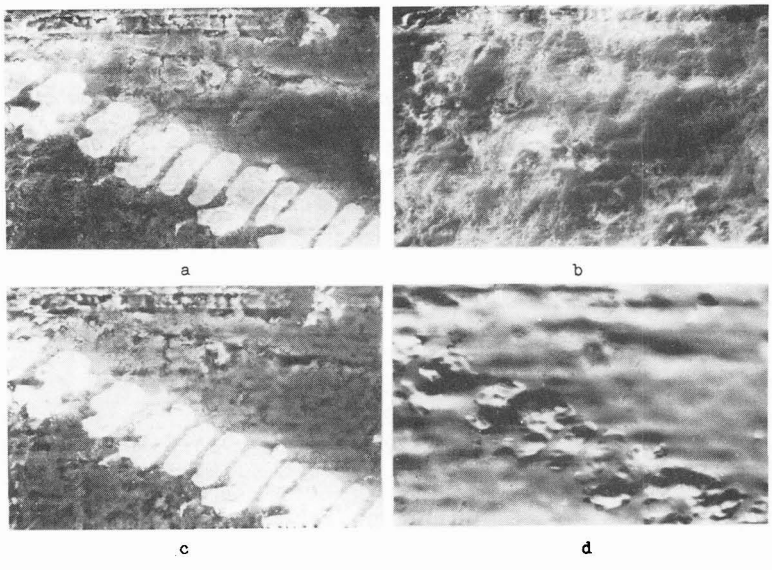

Fig.8 - Micrographs of a glass matrix with inclusions of circonium oxide obtained with the detector system of Fig.7. a) A+B SE mode with material and b) A-B SE with topographic contrast, c) A+B BSE mode with material contrast and d) A-B BSE with imaging artifacts at boundaries between low and high material.

boundary between low and high Z material. The A-B signal will be inverted when the sequence of the material is changed which results in a contrast similar to that one of a surface step.

Characteristic properties of the A±B SE and BSE signals obtainable with a two-detector system can be demonstrated by scanning across a sphere (steel ball) which represents all tilt and azimuth angles $\emptyset$, χ. When assuming the validity of Lambert's law equ.(2) and $\delta \propto \sec \emptyset$, the expected signals A and B can be calculated by summing over those SEs with exit momenta to the right and left, respectively. Such a calculation results in an A-B SE signal $\propto dz/dx$ where z is parallel to the electron beam and x in scan direction parallel to the interconnection of A and B. This can be verified by recording line-scans across the centre /19/ or of isodensities (Fig.9b). A comparison with the isodensities of a conventional one-detector system (Fig.9a) shows that the A-B signal (Fig.9b) results in a more unique correlation to $\emptyset$ and χ. An on-line analogue or digital integration of the A-B SE signal can restruct the surface profil z(x) for not too large tilt angles $\emptyset$.

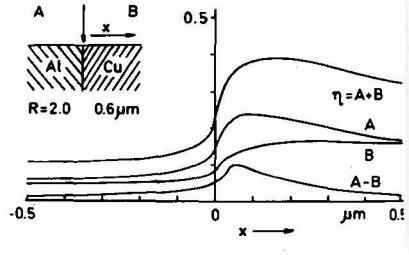

Fig.9 - BSE signal recorded by detectors A and B at a plane Al-Cu boundary

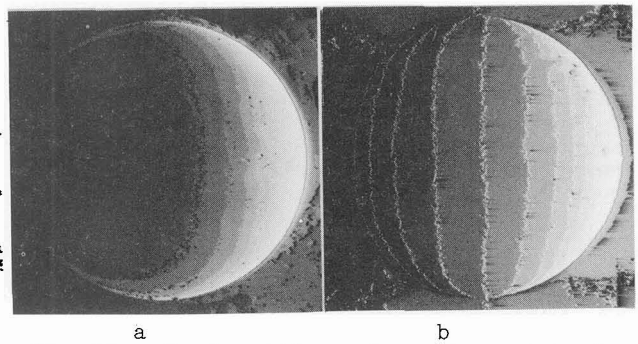

a b

Fig.10 - Isodensities of a sphere (steel ball, 1 mm $\emptyset$) for a) an one-detector and b) the A-B SE signal of a two-detector system.

The A+B BSE signal will be of interest for a quantitative record of material contrast. Line-scans across a sphere and isodensities show that the signal does not drop significantly until tilt angles $\emptyset$=40-50°. The signal can be used to measure a mean value $\bar{\eta}$ which results for a multicomponent specimen from the mass concentrations c_i and the backscattering coefficients η_i of the pure elements by $\bar{\eta} = \Sigma\, c_i \eta_i$ /20/. Or a mean atomic number $\bar{Z}$ can be evaluated which shows the same backscattering coefficient in the $\eta(Z)$ relation of Fig.5. Figure 10 shows a histogram of a four-element test specimen which was calibrated with copper and a polynomal fit of $\eta(Z)$.

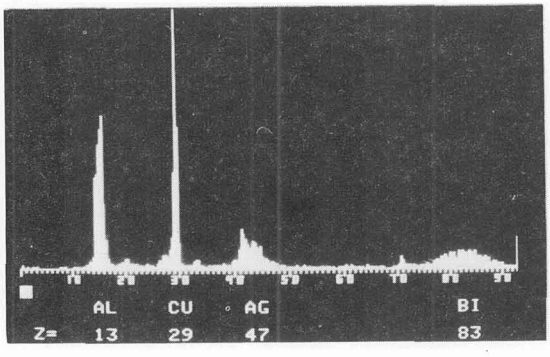

Fig.10 - Histogram of a four-element test specimen of Al, Cu, Ag and Bi transformed to a Z-distribution by calibrating the BSE signal for Cu and using a polynom fit of $\eta(Z)$.

Another possibility for separating material and topographic contrasts is to record the SE - k BSE signal when simultaneously recording the SE with an Everhart-Thornley detector and the BSE by scintillation detector /7/. This supposes that image structures generated by the second part δ_{BSE} in equ.(1) will be similar to those recorded by BSE.

III - Other types of contrast

A two-detector system cannot only separate material and topographic contrasts but also the type-1 magnetic contrast produced by the action of external magnetic stray fields on the SE trajectories and the crystal orientation or channelling contrast caused by differences in the back-scattering coefficient η due to electron channelling.

In type-1 magnetic contrast, the angular distribution equ.(2) is rotated around the y-axis by an angle $\Phi \propto \int B_y \, dz$. Therefore, this type of contrast can only be observed by an angular selection of the SE exit momenta. The use of the two-detector system results in an optimum contrast in the A-B SE mode /17/ and in the A+B SE mode this contrast will be cancelled. Because the collection conditions of the two-detector system are reproducible, a calibration of the signal A-B/A+B should be applicable for measuring $\int B_y \, dz$ more quantitatively.

For the observation of a good channelling contrast, it is necessary to have a plane and clean surface. For metals, it is very effective to use ion-beam etching with 10 keV argon ions, for example /21/. Then the channelling contrast can optimally be observed in the A+B SE and BSE modes and will be cancelled in the A-B modes. For example, the A-B SE mode only shows the topography produced by ion-beam etching.

References

/1/ REIMER L., Electron Microscopy 1982, Vol.1, 79, Frankfurt 1982
/2/ WELLS O.C., Scanning Electron Microscopy, p.133, McGraw Gill, New York 1974
/3/ BLASCHKE R., SCHUR K., Beitr.elektr.mikr.Direktabb.Oberfl. 5 (1972) 269
/4/ WELLS O.C., SEM 1978/I, 293, SEM Inc., AMF O'Hare 1978
/5/ REIMER L; PÖPPER W., BRÖCKER W., SEM 1978/I, 709, SEM Inc., AMF O'Hare 1978
/6/ KIMOTO S., HASHIMOTO H., The Electron Microprobe, p.480, John Wiley, New York 1966
/7/ REIMER L., VOLBERT B., Electron Microscopy 1980, Vol.3, 172, TheHague 1980; Philips Electron Optics Bull.118, Eindhoven 1982
/8/ REIMER L., SEM 1979/II, 111, SEM Inc., AMF OHare 1979
/9/ REIMER L., TOLLKAMP C., SCANNING 3 (1980) 35
/10/ LÖDDING B., REIMER L., Beitr.elektr.mikr. Direktabb.Oberfl. 14 (1981) 315
/11/ DRESCHER H., REIMER L., SEIDEL H., Z.angew.Physik 29 (1970) 331
/12/ BAUER, H.D., Exp.Techn.Physik 27 (1979) 331
/13/ HOFFMANN K.E., SCHMORANZER H., Electron Microscopy 1982, Vol.1, 205, Frankfurt 1982
/14/ SEILER H., Z.angew.Physik 22 (1967) 249
/15/ REIMER L., Optik 27 (1968) 86
/16/ REIMER L:, DRESCHER H., J.Phys. D 10 (1977) 805
/17/ VOLBERT B., REIMER L., SEM 1980/IV, 1, SEM Inc., AMF OHare 1980
/18/ REIMER L., VOLBERT B., Scanning 2 (1979) 238; Inst.Phys.Conf.Ser. No. 52, p.238, Bristol 1980
/19/ REIMER L., TOLLKAMP C., Electron Microscopy 1982, Vol.2, 543, Frankfurt 1982
/20/ CASTAING R., Adv.Electr. Electron Phys. 13 (1960) 317
/21/ HOFFMANN M., REIMER L., Scanning 4 (1980) 91